Обзор ArXiv/astro-ph, 6-11 апреля 2018 года

От Сильченко О.К.

Astro-ph: 1804.01546

Discovery of disc truncations above the galaxies' mid-plane in Milky Way-like galaxies

Cristina Martínez-Lombilla,[1,2⋆] Ignacio Trujillo[1,2] and Johan H. Knapen[1,2]
[1] *Instituto de Astrofísica de Canarias (IAC), La Laguna, 38205, Spain*
[2] *Departamento de Astrofísica, Universidad de La Laguna (ULL), E-38200, La Laguna, Spain*

Accepted XXX. Received YYY; in original form ZZZ

ABSTRACT

Disc truncations are the closest feature to an edge that galaxies have, but the nature of this phenomena is not yet understood. In this paper we explore the truncations in two nearby (D ~15 Mpc) Milky Way-like galaxies: NGC 4565 and NGC 5907. We cover a wide wavelength range from the NUV and optical, to 3.6 μm. We find that the radius of the truncation (26±0.5 kpc) is independent of wavelength. Surprisingly, we identify (at all wavelengths) the truncation at altitudes as high as 3 kpc above the mid-plane, which implies that the thin disc in those outer regions has a width of at least this value. We find the characteristic U-shape radial colour profile associated with a star formation threshold at the location of the truncation. Further supporting such an origin, the stellar mass density at the position of the truncation is ~1-2 $M_{\odot}$ pc^{-2}, in

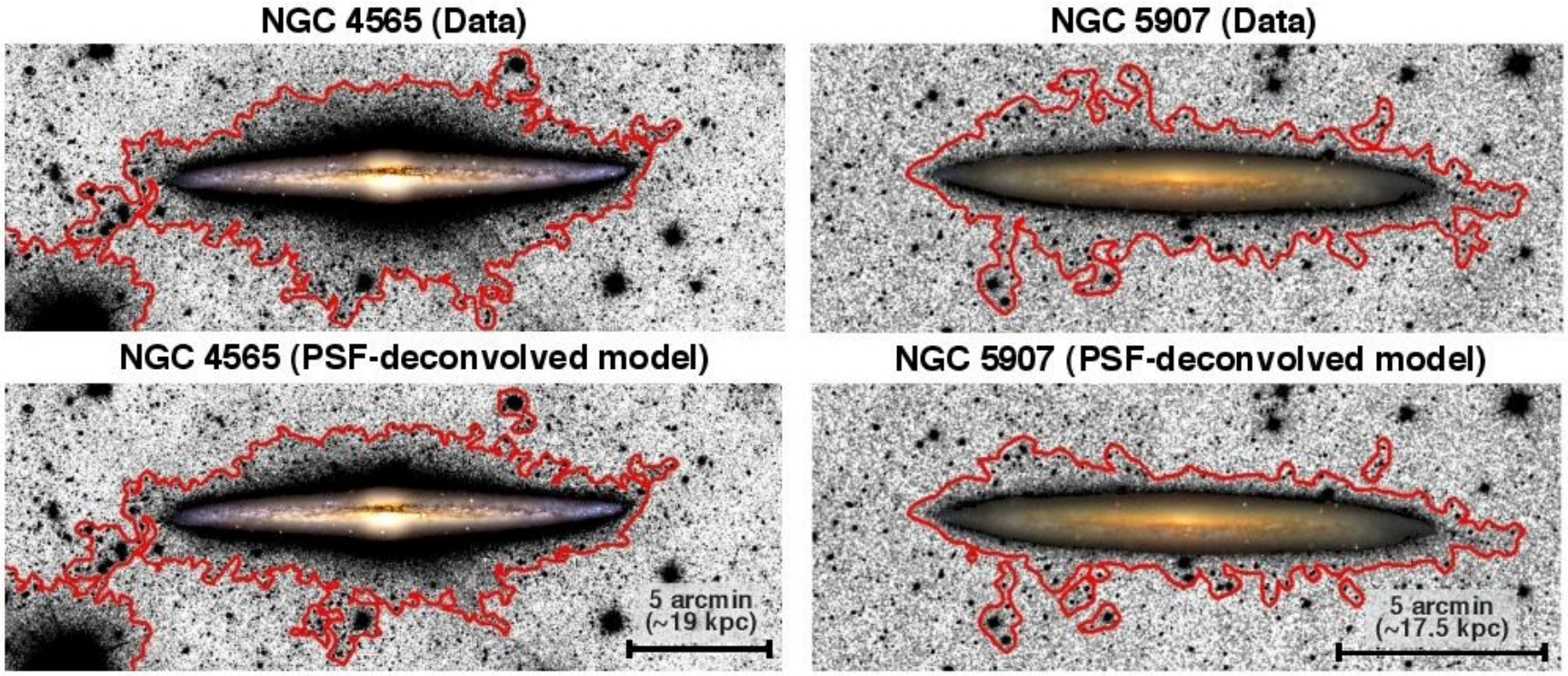

Figure 1. Images of NGC 5907 (left) and NGC 4565 (right) in SDSS *gri* combined light (roughly equivalent to a deep r-band image). For illustrative purposes, a colour image obtained with the same telescope has been inserted atop the saturated disc region of the galaxy. Panels in the first row show the observed data and the second row are the PSF deconvolved models for each galaxy (see Sect. 3.4 for details). Overplotted on all the images are the surface brightness contours (red lines) corresponding to 27 mag arcsec^{-2}.

Резали фотометрическими щелями изображения GALEX, SDSS, S4G

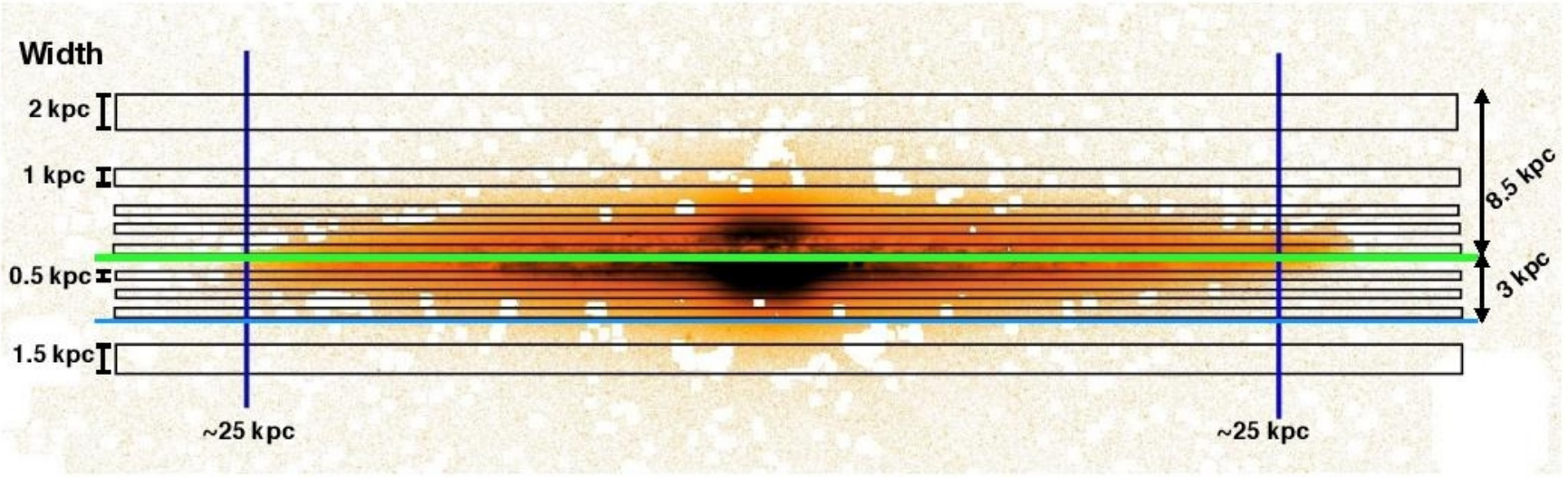

Figure 3. Image of NGC 4565 in the SDSS *gri* combined band. The green horizontal line covers the region along which we obtain the galaxy mid-plane radial surface brightness profile. The black rectangles show the locations where the radial surface brightness profiles above and below the galaxy mid-plane were extracted. The numbers on the left are the widths of each profile. The numbers on the right are (1) the highest altitude we reach (8.5 kpc) and (2) the height up to where we are able to detect the truncation (3 kpc) which is indicated with the horizontal blue line. The vertical dark blue lines point out a radial distance of 25±0.4 kpc from the centre of the galaxy. The truncation for this galaxy is located at ~26.6 kpc.

Профили в разных длиных волн

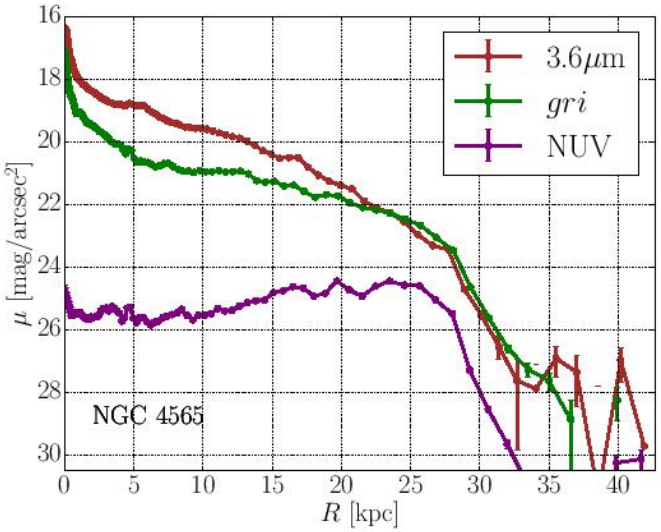

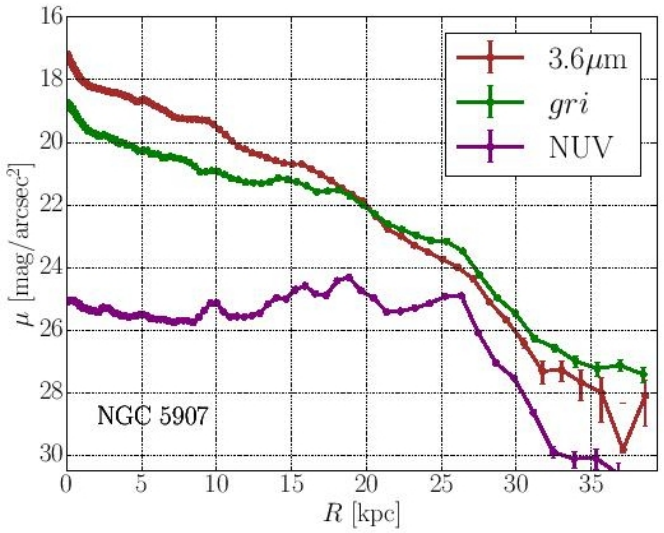

Figure 5. Surface brightness profiles along the disc mid-plane of NGC 4565 (up) and NGC 5907 (down) in the three wavelength ranges (UV/optical/NIR).

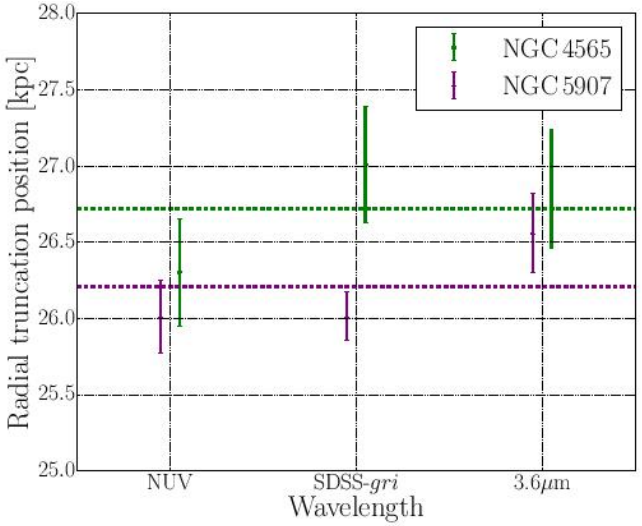

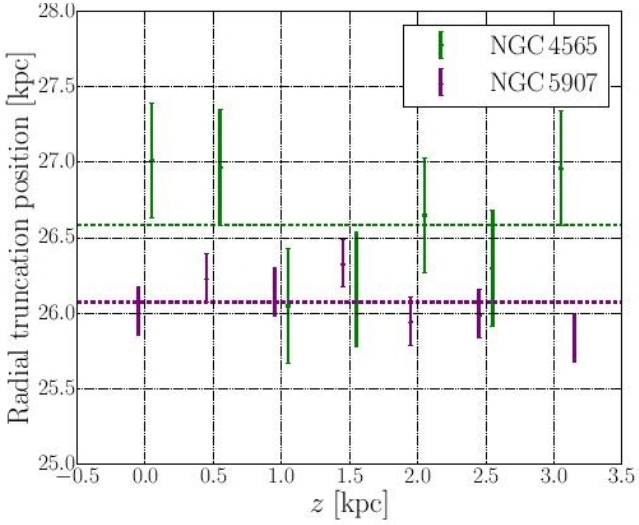

Figure 6. Truncation position at each wavelength, measured from the SB profiles along the disc plane (above) and at different heights in the SDSS-gri combined band (bottom). In both cases the dashed lines represent the mean value of the points in the corresponding colour.

Положение обрыва не меняется с длиной волны и высотой над плоскостью !

Профили цвета

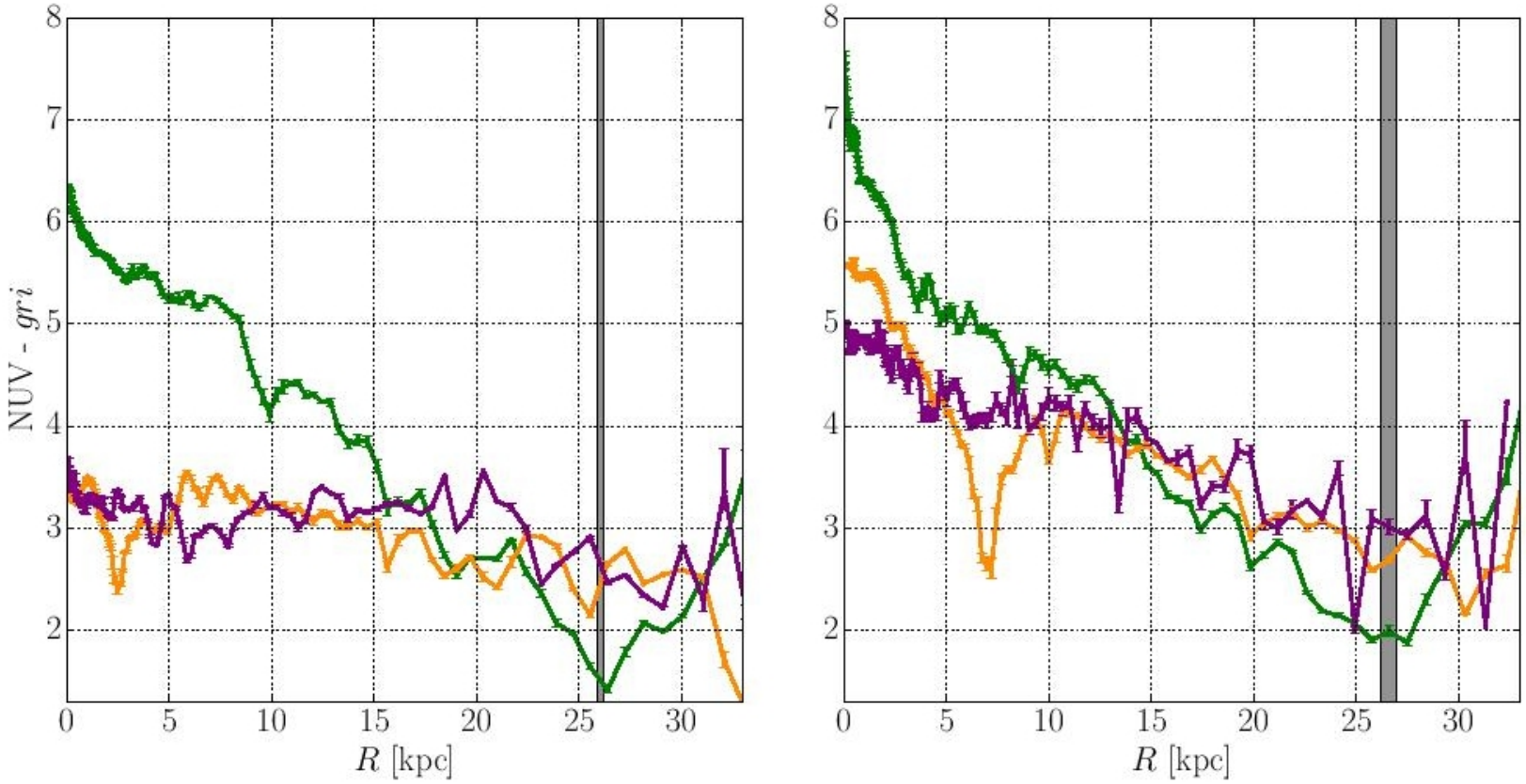

Figure 7. Radial colour profiles for both galaxies along their mid-plane, at 1.5 kpc and at 3 kpc height (NGC 5907 at left and NGC 4565 at right). The rows show the different colours: *gri* - 3.6μm in the top row and NUV - *gri* in the bottom. The vertical dark grey regions of each galaxy represent the mean position of the truncations for all the heights in the SDSS-*gri* combined band, plus/minus the standard deviation of that distribution of truncation positions: 26.1±0.2 kpc for NGC 5907 and 26.6±0.4 kpc for NGC 4565.

Верхний предел на скорость радиального роста диска <0.5 kpc/Gyr

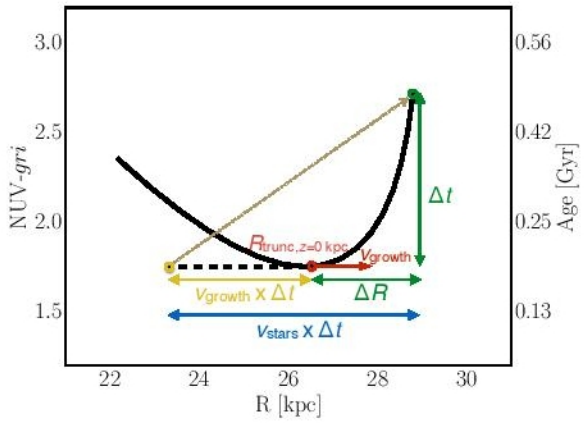

Figure 10. A cartoon illustrating how to use the shape of the radial colour profile beyond the truncation to estimate the growth speed $v_{\rm growth}$ of a disc. The observables in the radial colour profile beyond the truncation are Δt and ΔR. In this particular example we use the colour NUV-r (vertical left axis) as a proxy to measure the interval of time (vertical right axis). The yellow dot indicates the birth location of a star in the colour-radial distance plane. The green dot is the current position of the star born at the yellow dot location. The red dot is the position of the truncation.

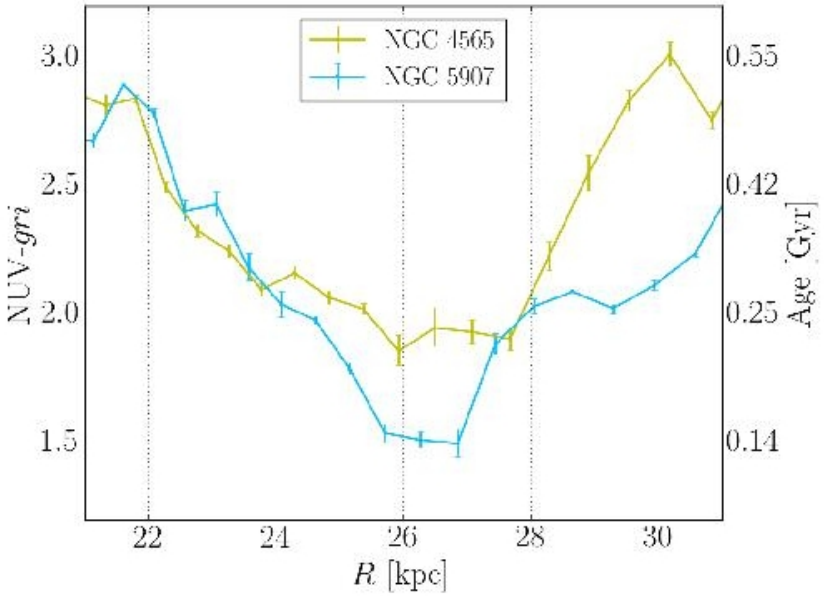

Figure 9. A zoom in to the location of the truncation in the NUV-*gri* colour versus radial location plane.

Astro-ph: 1804.02402

SPATIALLY RESOLVED STELLAR KINEMATICS FROM LEGA-C: INCREASED ROTATIONAL SUPPORT IN $Z\sim0.8$ QUIESCENT GALAXIES

Rachel Bezanson,[1,2] Arjen van der Wel,[3,4] Camilla Pacifici,[5] Kai Noeske,[4] Ivana Barišić,[4] Eric F. Bell,[6] Gabriel B. Brammer,[5] Joao Calhau,[7] Priscilla Chauke,[4] Pieter van Dokkum,[8] Marijn Franx,[9] Anna Gallazzi,[10] Josha van Houdt,[4] Ivo Labbé,[9] Michael V. Maseda,[9] Juan Carlos Muños-Mateos,[11] Adam Muzzin,[12] Jesse van de Sande,[13] David Sobral,[7,9] Caroline Straatman,[3] and Po-Feng Wu[4]

[1] *Department of Physics and Astronomy and PITT PACC, University of Pittsburgh, Pittsburgh, PA, 15260, USA*
[2] *Department of Astrophysics, Princeton University, Princeton, NJ 08544, USA*
[3] *Sterrenkundig Observatorium, Universiteit Gent, Krijgslaan 281 S9, B-9000 Gent, Belgium*
[4] *Max-Planck Institut für Astronomie, Königstuhl 17, D-69117, Heidelberg, Germany*
[5] *Space Telescope Science Institute, 3700 San Martin Drive, Baltimore, MD 21218, USA*
[6] *Department of Astronomy, University of Michigan, 1085 South University Ave., Ann Arbor, MI 48109, USA*
[7] *Department of Physics, Lancaster University, Lancaster LA1 4YB, UK*
[8] *Astronomy Department, Yale University, New Haven, CT 06511, USA*
[9] *Leiden Observatory, Leiden University, P.O.Box 9513, NL-2300 AA Leiden, The Netherlands*
[10] *INAF-Osservatorio Astrofisico di Arcetri, Largo Enrico Fermi 5, I-50125 Firenze, Italy*
[11] *European Southern Observatory, Alonso de Crdova 3107, Casilla 19001, Vitacura, Santiago, Chile*
[12] *Department of Physics and Astronomy, York University, 4700 Keele St., Toronto, Ontario, Canada, MJ3 1P3*
[13] *Sydney Institute for Astronomy, School of Physics, A28, The University of Sydney, NSW, 2006, Australia*

Multi-slit спектральный обзор

2.1. *The LEGA-C Spectroscopic Survey*

The spectroscopic data included in this analysis are drawn from the first year data release of the Large Early Galaxy Astrophysics Census (LEGA-C) survey (van der Wel et al. 2016). This project is a 128-night ESO Public Spectroscopic survey of massive galaxies at $0.6 < z < 1.0$ in the COSMOS field using VIMOS on the VLT. The LEGA-C Survey primary sample of $\sim$ 3000 galaxies is selected with a photometric or spectroscopic redshift-dependent K-magnitude limit ($K = 20.7-7.5\times\log((1+z)/1.8)$), corresponding to a representative sampling of galaxy colors down to $\log M_\star/M_\odot \gtrsim 10.4$. The defining, unique aspect of the LEGA-C spectra is the deep 20-hour long integration at a resolution of $R = 2500$ in the wavelength range $\sim$6300 − 8800Å. The first year dataset consists of 7 masks of roughly 130 galaxies in each mask with slits that are oriented in the N-S direction. The combined data yield the extremely high signal-to-noise $S/N \sim 20\text{Å}^{-1}$ in the continuum. The data reduction procedure is described by van der Wel et al. (2016). Two-dimensional and extracted one-dimensional reduced spectra are publicly available via the ESO Science Archive Facility.

Отбор галактик без звездообразования

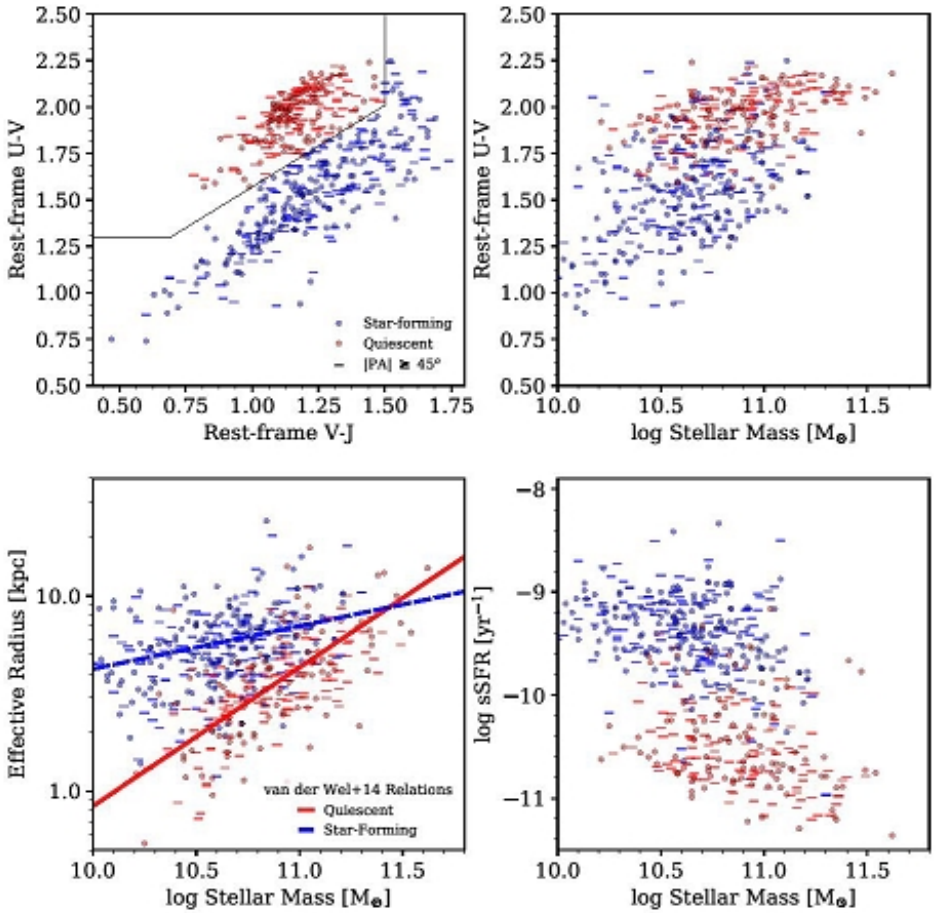

Figure 1. Properties of the complete LEGA-C year one dataset. Symbol colors differentiate between star-forming (blue) and quiescent (red) galaxies as determined by U-V and V-J rest-frame colors and cuts from Muzzin et al. (2013b) (upper left panel). Misaligned galaxies ($|PA| \geq 45°$) are excluded from this study and are indicated by horizontal lines. Star-forming and quiescent galaxies in the LEGA-C sample have different distributions in color (upper right panel), physical size (bottom left panel), and sSFR (bottom right panel); for this study we focus on the kinematics of the quiescent population.

Примеры спектров

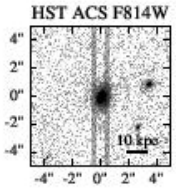

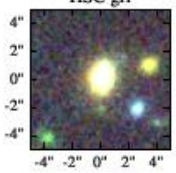

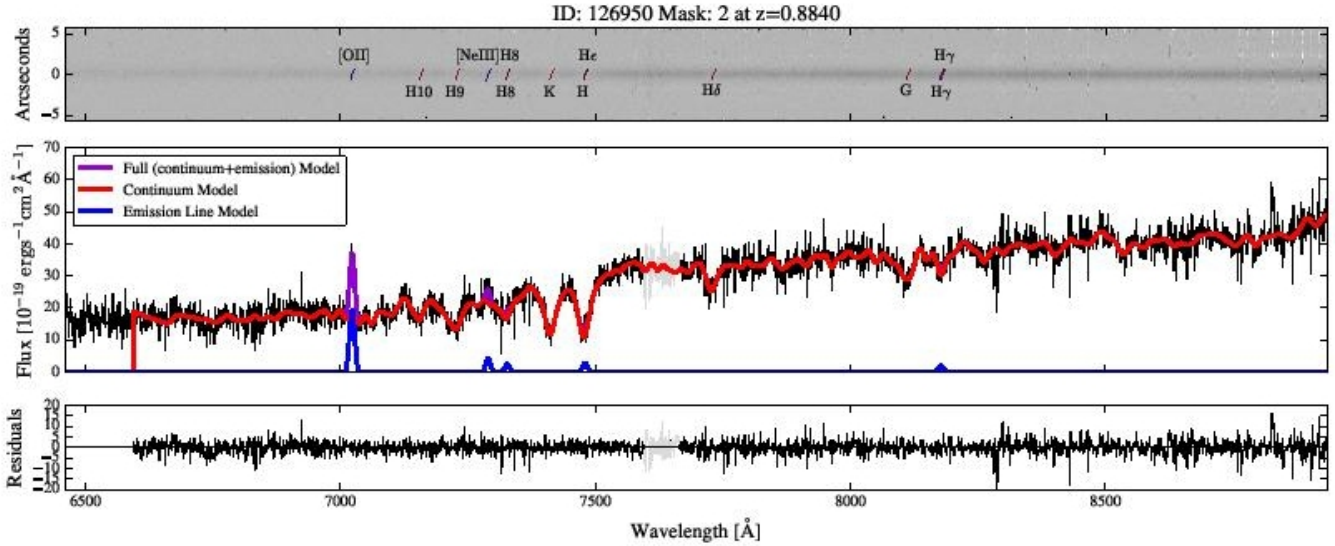

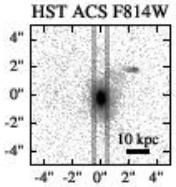

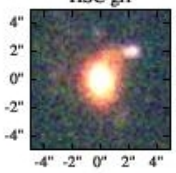

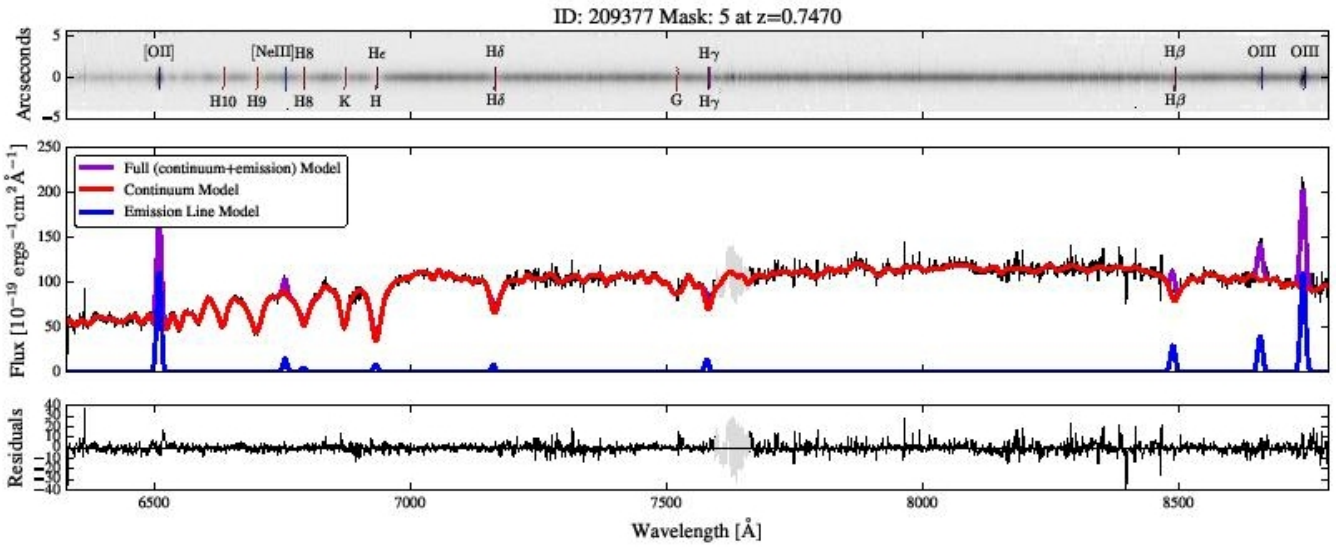

Кинематика для этих галактик

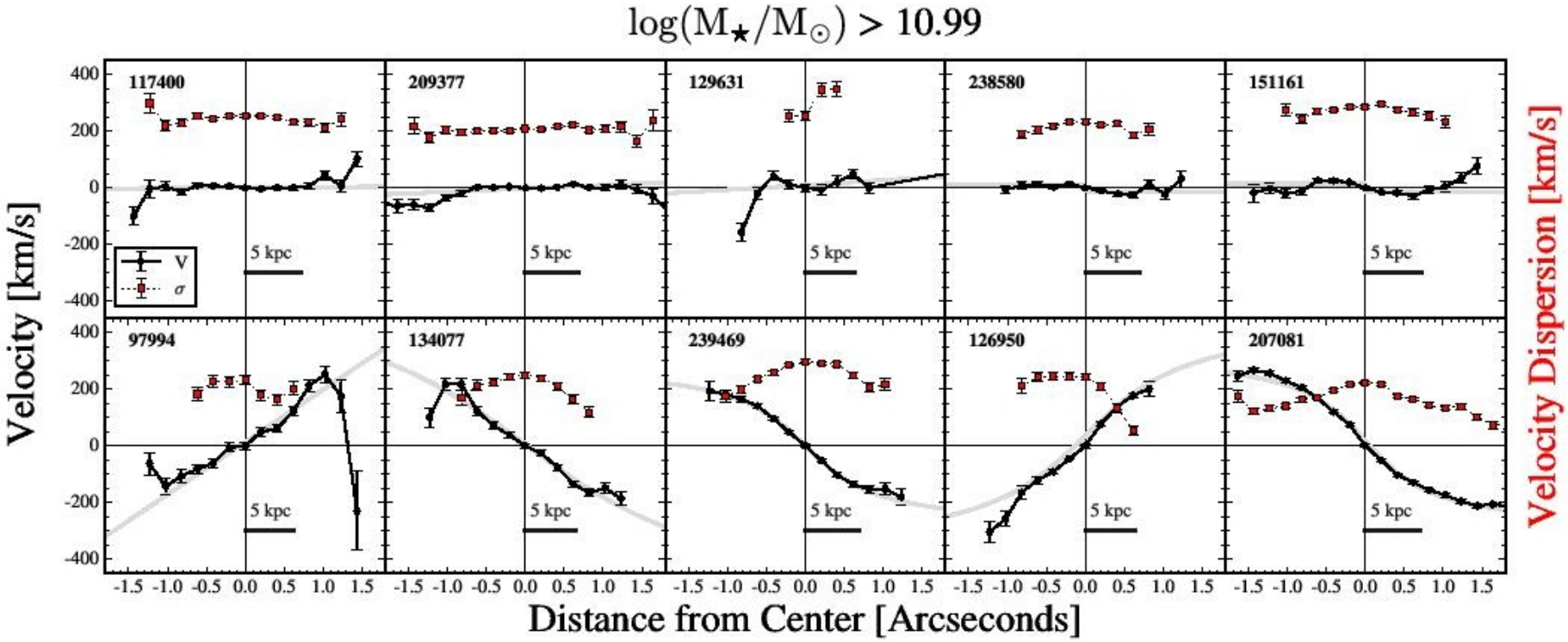

Диаграмма Бинни-Корменди

Therefore in addition to $|V_5|/\sigma_0$, we introduce $(V_5/\sigma_0)^*$ following e.g. Binney (1978); Davies et al. (1983), which is defined as the V/σ normalized by the $(V/\sigma)_O$ for an oblate, isotropic model and should be largely independent of projection effects. We adopt the approximation $V/\sigma \approx \sqrt{\epsilon/(1-\epsilon)}$ from Kormendy (1982). Following this definition,

$$(V_5/\sigma_0)^* = \frac{(|V_5|/\sigma_0)}{\sqrt{\epsilon/(1-\epsilon)}}. \qquad (1)$$

Корреляции всякие

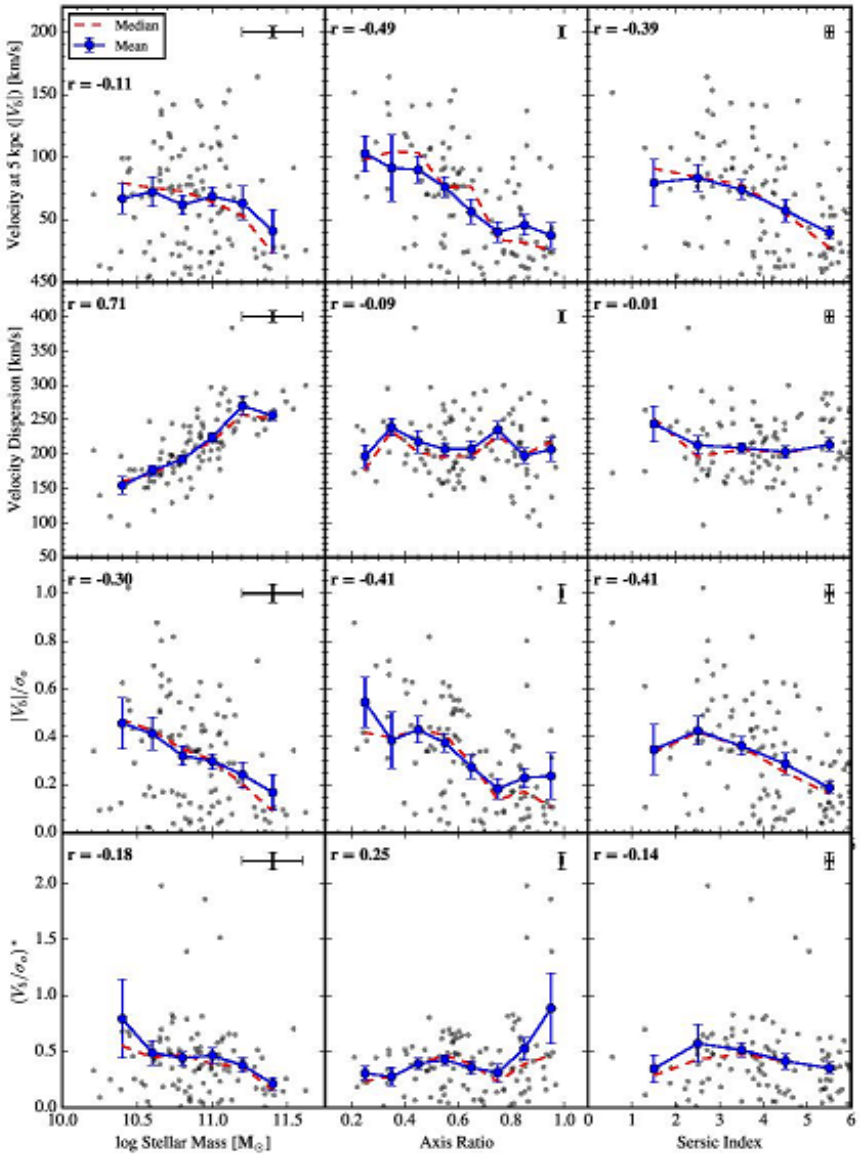

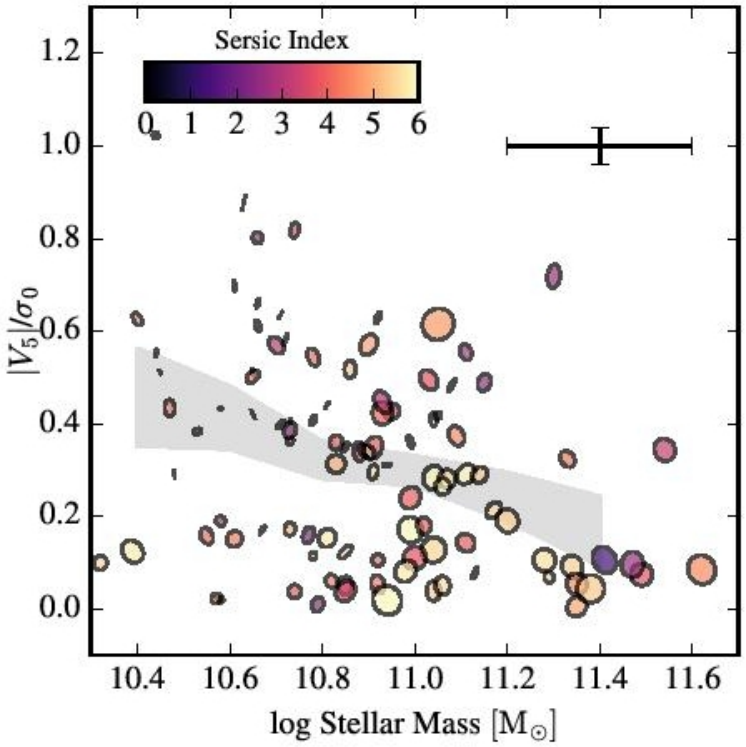

Figure 5. Rotational support ($|V_5|/\sigma_0$) versus stellar mass for the LEGA-C sample of massive, quiescent galaxies. Symbol size indicates the galaxy effective radii (in log scale) and position angles and axis ratios of symbol ellipses reflect those of the galaxies. Symbol color indicates Sérsic index. The mean relation is indicated by gray band and average uncertainty is indicated by errorbars in the upper right corner. The majority of high-mass galaxies have minimal rotational support, even when their Sérsic indices are disk-like, how-

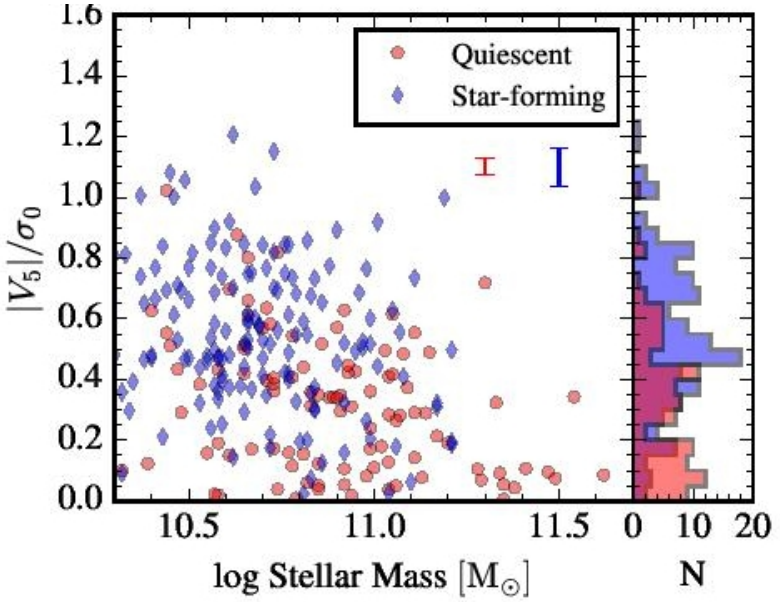

Figure 6. Observed rotational support of LEGA-C galaxies versus stellar mass for star-forming (blue diamonds) and quiescent galaxies (red circles). Average uncertainties, shown as blue and red errorbars in the upper right, are higher for the star-forming galaxies (~ 0.1) than for quiescent galaxies (~ 0.04) in the LEGA-C sample. The right panel indicates the histograms in rotational support between the star-forming and quiescent populations; the distributions are overlapping but on average star-forming galaxies show higher V_5/σ_0 than quiescent galaxies overall and at fixed mass.

Сравнение с CALIFA – z=0

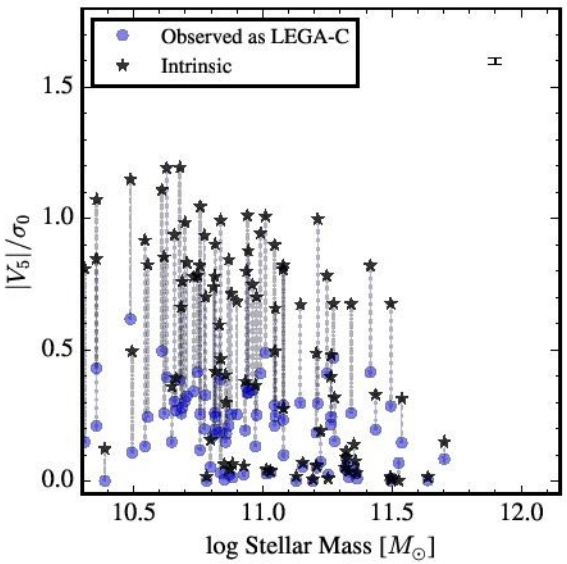

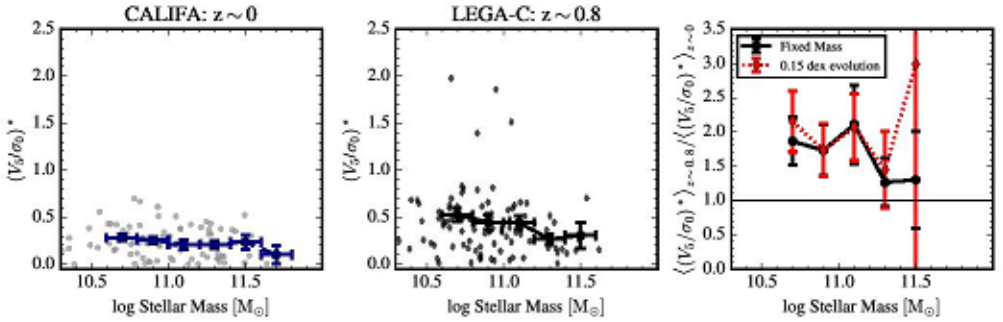

Figure 12. Rotational support ($(V_5/\sigma_0)^*$) versus stellar mass for the simulated CALIFA $z \sim 0$ galaxies (left panel), LEGA-C galaxies at $z \sim 0.8$ (center panel), and the ratio of the averages (right panel). At the highest mass end ($\log M_*/M_\odot \gtrsim 11.25$) the rotational support is very similar, but at lower masses, the LEGA-C sample exhibits similar or slightly more rotational support than CALIFA galaxies at fixed mass (black symbols and solid line in the right panel). However, when compared to more massive descendants (red symbols and dashed line, assuming 0.15 dex evolution) galaxies at $z \sim 0.8$ exhibit $50 - 100\%$ higher rotational support than local galaxies.

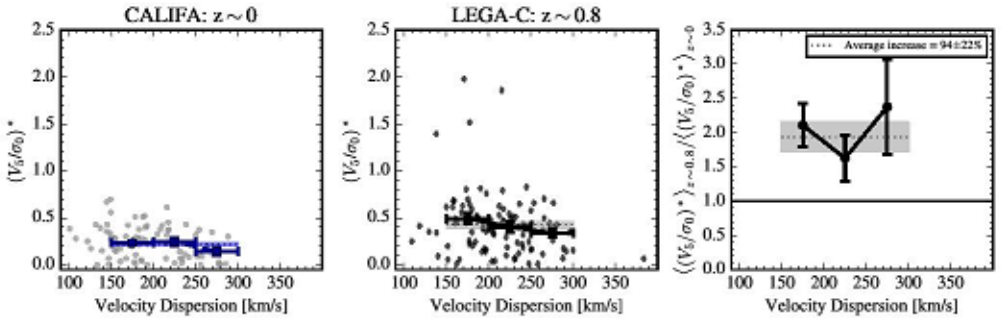

Figure 13. Rotational support ($(V_5/\sigma_0)*$) versus central velocity dispersion (σ_0) for the simulated CALIFA $z \sim 0$ galaxies (left panel), LEGA-C galaxies at $z \sim 0.8$ (center panel), and the ratio of the averages (right panel). In each panel individual galaxies are indicated by small symbols, larger black circles indicate the running averages and jackknife uncertainties, and the horizontal bands indicate the average value and uncertainty evaluated between $150 < \sigma < 300$ km/s. At fixed central velocity dispersion, which is likely more stable than stellar mass, the higher redshift galaxies exhibit more rotational support than their local counterparts by a factor of $\sim 1.5 - 2$.

Astro-ph: 1804.01581

A Test of MONDian Gravity in ∼300 pressure supported elliptical galaxies from the MaNGA survey

R. Durazo[1], X. Hernandez[1], B. Cervantes Sodi[2] and S. F. Sanchez[1]

[1]*Instituto de Astronomía, Universidad Nacional Autónoma de México, Apartado Postal 70–264 C.P. 04510 México D.F. México.*

[2]*Instituto de Radioastronomía y Astrofísica, Universidad Nacional Autonoma de México, Campus Morelia, 58090 Morelia, Michoacán, México.*

ABSTRACT

Pressure supported systems modeled under MONDian extended gravity are expected to show an outer flattening in their velocity dispersion profiles. A characteristic scaling between the amplitude of the asymptotic velocity dispersion and the radius at which the flattening occurs is also expected. By comprehensively analyzing the dynamical behavior of ∼300 extremely low rotating elliptical galaxies from the MaNGA survey, we show this type of pressure supported systems to be consistent with MONDian expectations, for a range of central velocity dispersion values of $60km/s < \sigma_{central} < 280km/s$ and asymptotic velocity dispersion values of $28km/s < \sigma_{\infty} < 250km/s$. We find that a universal velocity dispersion profile accurately describes the studied systems; the predicted kinematics of extended gravity are verified for all well observed galaxies.

MOND!

2. MONDian Theoretical expectations

In order to model observed galactic dynamics assuming only baryonic matter, a change from the Newtonian force law $F_N = GM/r^2$ to a MONDian force law $F_M = (GMa_0)^{1/2}/r$ is needed at a scale of $R_M = (GM/a_0)^{1/2}$ e.g. Milgrom (1983). Most authors seem to agree on a relatively abrupt transition between the above regimes, from studies on Milky Way rotation curve comparisons e.g. Famaey & Binney (2005), solar system dynamics e.g. Mendoza et al. (2011) and Galactic globular cluster modeling e.g. Hernandez et al. (2012).

Centrifugal equilibrium velocities will show a Tully-Fisher value in the MONDian regime of:

$$V = (GMa_0)^{1/4}, \tag{1}$$

for a test particle orbiting a total baryonic mass M. In the modified gravity region, centrifugal equilibrium velocities and isotropic velocity dispersions will yield a slightly different scaling with respect to the Newtonian case, namely:

$$\sigma_\infty = V/\sqrt{3}, \tag{2}$$

where σ_∞ is the asymptotic velocity dispersion, e.g. Milgrom (1984), Hernandez & Jimenez (2012). Consequently, the isotropic Maxwellian velocity dispersion of a pressure supported system in the modified gravity domain can be expressed as:

$$\sigma_\infty^2 = \frac{1}{3}(GMa_0)^{1/2}. \tag{3}$$

$$R_M = \frac{3\sigma_\infty^2}{a_0}, \tag{4}$$

which in astrophysical units results in:

$$\left(\frac{R_M}{pc}\right) = 0.81\left(\frac{\sigma_\infty}{km/s}\right)^2. \tag{5}$$

Equation (5) now links two directly observable features of the velocity dispersion profile of a pressure supported system, where σ_∞ is the asymptotic projected velocity dispersion at large radii and R_M is the characteristic radius at which the velocity dispersion profile begins to flatten. For

Профили дисперсии скоростей

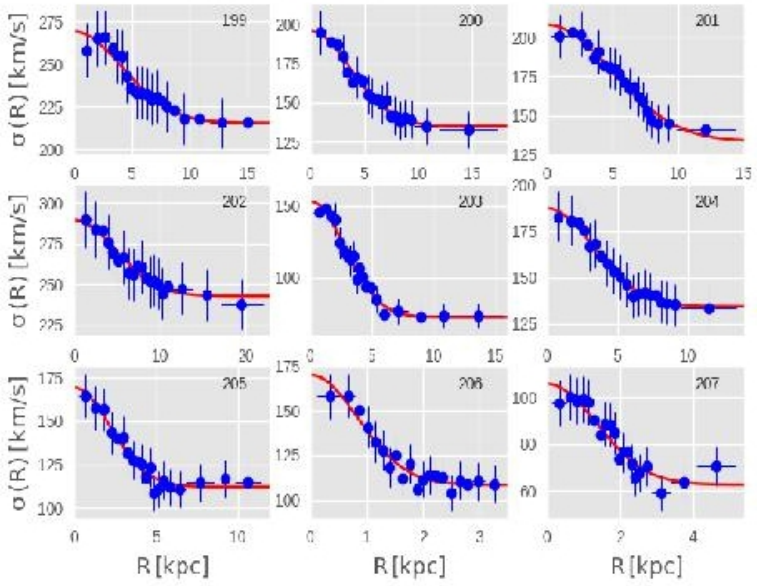

Fig. 1.— A random selection of 9 fitted velocity dispersion profiles from our larger sample. Blue dots represent the averaged velocity dispersion observations with horizontal error bars delimiting each radial bin, and vertical error bars representing the averaged empirical errors. The red curves are the fits to eq. (6).

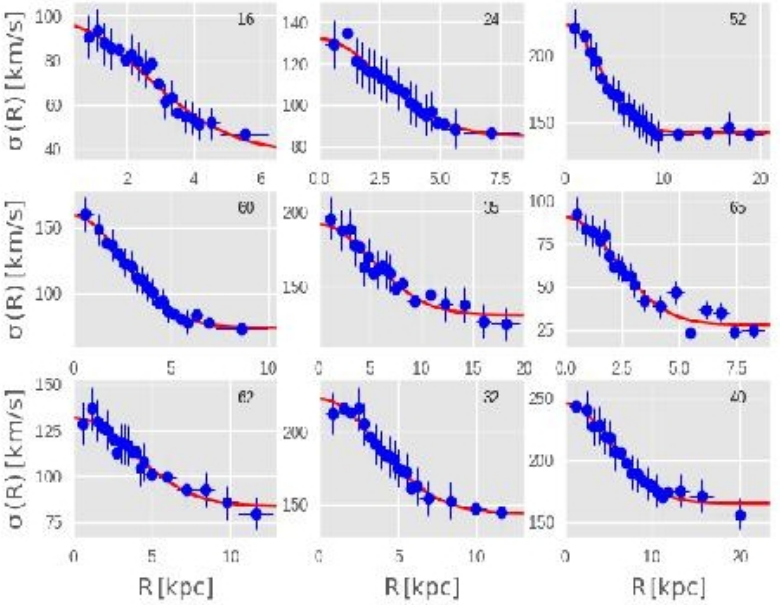

Fig. 2.— A random selection of 9 fitted velocity dispersion profiles from our lowest relative error sub sample. Blue dots represent the averaged velocity dispersion observations with horizontal error bars delimiting each radial bin, and vertical error bars representing the propagated empirical errors. The red curves are the fit to eq. (6).

Проверка MOND – работает!

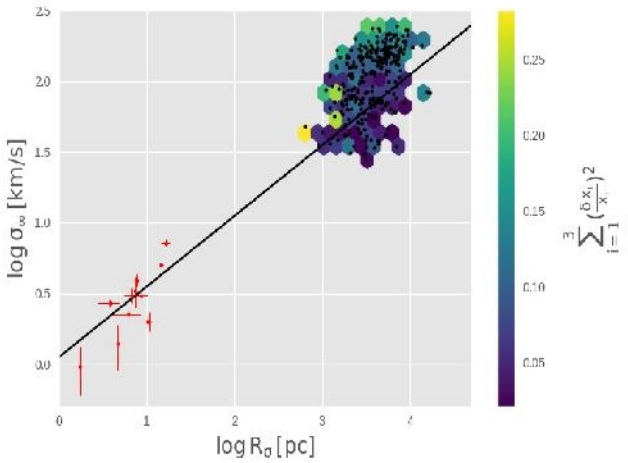

Fig. 6.— σ_∞ vs R_σ values for our larger sample of 292 low rotating ellipticals. The color palette represents the third plotted variable, the total sum of the relative errors of the fitted parameters. The black dots show the actual sample distribution. Points at the lower left of the plot show the GC velocity profiles studied in Durazo et al. (2017). The solid line is not a fit to the data, but actually shows the MONDian expectations of equation (4) for the predicted scaling of $R_M = 3\sigma_\infty^2/a_0$, $R_M/pc = 0.81(\sigma_\infty/kms^{-1})^2$

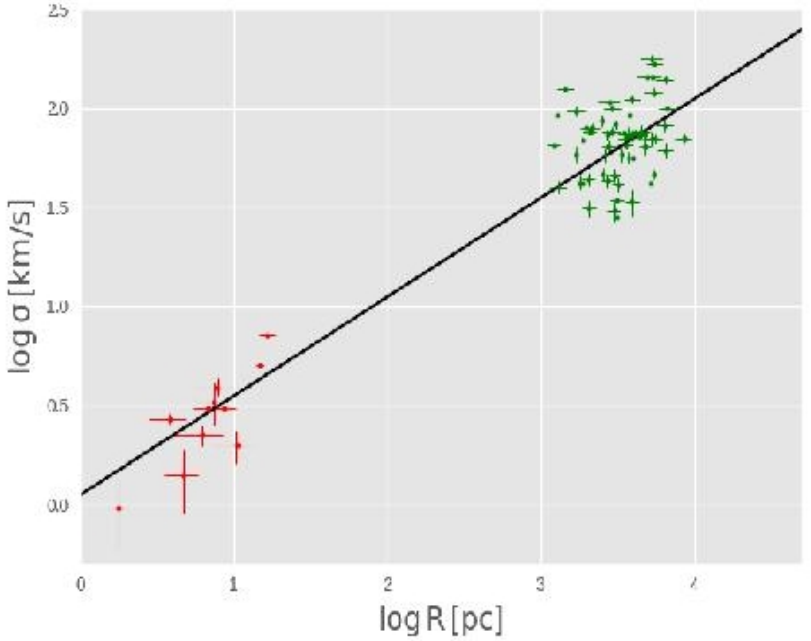

Fig. 7.— σ_∞ vs R_σ values for our sub-sample of the first quintile of lowest summed relative errors. Points at the lower left of the plot show the GC velocity profiles studied in Durazo et al. (2017). The solid line is not a fit to the data, but actually shows the MONDian expectations of equation (4) for the predicted scaling of $R_M = 3\sigma_\infty^2/a_0$, $R_M/pc = 0.81(\sigma_\infty/kms^{-1})^2$ through the identification of $R_\sigma = R_M$.

EWASS-2018, Ливерпуль

- SS30 – будущие спектрографы интегрального поля

HIRES/ELT (Marconi A.)

- R~100000, range 0.37-2.4 mkm (0.4 – 1.8?)
- Два рукава, оптический и инфракрасный, VIS & NIS
- Щель запитывается ПУЧКАМИ световодов.
- В приоритете – экзопланеты; но и ранняя Вселенная тоже

HARMONI/ELT (M. Tecza)

- IFU - «Рабочая лошадка» ELT
- Range 0.47-2.45 mkm
- R ~ 3300, 7000, 17000; одна решетка (R=3300) на оптику и 10(!) на NIR
- Spaxels: 60x30 mas, 20 mas … 4 mas
- Slicer: 152 slices x 206 spaxels, максимальное поле 9’’x6’’, развод на 8 приемников.
- Ожидаемый предел R(AB)=25.6, H(AB)=27.0

MEGARA/GTC (A. Gil de Paz)

- Поле пучка фиберов 2.5’’x11.3’’
- На пучке – массив шестиугольных микролинз
- Spaxel 0.62’’
- Робот-позиционер, ездит по полю до 3.5’
- Диапазон – полный оптический, до 1 мкм
- Три спектральных разрешения – 5000, 13000 и 20000 (2 решетки на NIR)
- Эффективность от 15% до 25% (последнее – на 6000 A с разрешением 5000)